PART A

Design-Studies of a Van de Graaff Accelerator

PART A

Design-Studies of a Van de Graaff Accelerator

Contents

1. Introduction 6

2. A Review of the Development of Van de Graaff Generators 8

3. Choice of Insulator and Charge Transport Belt 11

4. Development of a Generating Voltmeter .. 14

5. Construction of the Pressurised Van de Graaff Generator 18

6. Studies on Charge Transport .. 20

7. Operational Characteristics of the Pressurised Van de Graaff Generator .. 26

8. Operation as a Test Accelerator .. 34

References 36

PART A

Design-Studies of a Van de Graaff Accelerator

1. Introduction

The design-studies of a small pressurised horizontal Van de Graaff accelerator in the one million volt range using indigenous materials are discussed in this part.

In § 2 the development of Van de Graaff generators from its early days are briefly reviewed. Our work started with the search for suitable indigenous materials for the insulating support and the charge transport belt. The results of the surface resistivity measurements of some indigenous materials carried out for this purpose are presented in § 3. Of all the materials studied perspex having a high surface resistivity $\sim 6 \times 10^{11}$ ohms/square was chosen as the insulating support structure material. Endless nylon woven belt was selected as the charge transport belt.

We next turned our attention to the development of a generating voltmeter for monitoring the terminal voltage of the Van de Graaff generator. Studies undertaken in this connection are described in § 4. In § 5 we discuss the constructional details of the Van de Graaff generator. We then investigated the conditions for optimum charge transport to the high voltage terminal. The results of this study are summarized in § 6. From these studies a suitable arrangement of combs with an optimum

geometry was selected out to obtain a charge carrying efficiency $\sim$ 75% of theoretical maximum.

In § 7 we present the operational characteristics of the generator under pressurised nitrogen gas. A maximum terminal voltage of 1.1 MV was achieved at a nitrogen gas pressure of 6 atmospheres absolute with a spray voltage of 38 KV. Finally in § 8 we describe the operation of the Van de Graaff generator as a test accelerator.

2. A Review of the Development of Van de Graaff Generators

The first Van de Graaff generator set up at Princeton was reported by R. J. Van de Graaff in 1931 (3). In this machine a silk belt 2½" wide was carried by two pulleys, one at ground potential which was powered by an electric motor, and the second inside a metal sphere of 24" diameter. The sphere was supported by glass rods. Charge from a row of needle points held at a positive potential of about 10 KV was sprayed as corona current onto the belt surface just after it left the grounded pulley. Charge was removed from the belt by a second row of needle points well within the sphere before the belt reached the inner pulley. Here electric fields are only negligibly affected by charge on the outer surface of the sphere regardless of the potential of the sphere.

Larger machines were built, notably the 1.2 MV generator at the Department of Terrestrial Magnetism (DTM) in the Carnegie Institute in Washington, D.C. by Tuve and others (17). However, it soon became clear that a new form of insulation would be required if higher voltages were to be obtained in an apparatus of managable size. G. G. Havens and R. G. Herb at Wisconsin first experimented with vacuum insulation (1,2), but this was soon given up in favour of high pressure gas. A really significant advance was made by Herb et al. in 1937 (15) with their horizontal pressurised generator, which accelerated protons to about 2.5 MeV. The tank was 22 ft. long and 5½ ft. in diameter. The insulation

was achieved with air at about 7 atmospheres pressure to which some CCl_4 was added.

A very significant event in the field of Van de Graaff generator technology was the formation of the High Voltage Engineering Corporation (HVEC) by R. J. Van de Graaff and his associates in 1947. The creation of HVEC made possible the construction of electrostatic generators to the highest engineering standards.

The next important achievement in this field is the successful development of tandem accelerators (18,19). In these accelerators negative ions are accelerated from the ground potential to the high voltage terminal where they are stripped of electrons and become positive ions. These positive ions are then accelerated to the ground potential. Thus the energy of the accelerated ions is doubled.

An alternative approach to the construction of high voltage electrostatic accelerators has been taken by the National Electrostatics Corporation (NEC) founded by R. G. Herb in 1965. They are using the so called Pelletron charging chains to replace the Van de Graaff belt. These are chains consisting of alternate mild steel cylinders separated by nylon insulating links. The metallic links are charged by induction for both up and down charging. They have marked advantages in terms of lifetime, reliability, and terminal voltage stability.

An important modification of the pelletron charging system in recent years was undertaken by Daresbury Research Laboratories (20). Here the charging chain is made up of a pair of pelletrons in which corresponding elements are connected by a conducting bar and hence the machine is known as Laddatron. This results in an increased current transfer to the high voltage terminal.

The main disadvantages of pelletron type generators are those of limited current carrying capacity and limited power transmission capability to the high voltage terminal. In view of these and the fact that the belt type of generators are easier to construct we decided to construct a belt type of Van de Graaff accelerator.

3. Choice of Insulator and Charge Transport Belt

Two important components for the production of high voltage in a Van de Graaff generator are the materials for the insulating support and the charge transport belt. Since the effective resistances of insulating materials are determined practically by their surface resistivities, we measured the surface resistivities of all available materials that can be used as structural supports and charge transport belt (4). The result of the study is summarized in tables 3.1 and 3.2.

Of all the materials studied, perspex, having a high surface resistivity $\sim 6 \times 10^{11}$ ohms/square, was chosen as the insulating support structure material because it was readily available and could be easily machined. The belt material besides having high surface resistivity, must also be capable of transmitting about 1 KW of power to the high voltage terminal at a rotational speed of about 5,000 linear ft/min. Endless nylon woven belts meet the above requirements and was selected for use in our generator.

However, the nylon belts were found to absorb moisture when left to humid atmospheres decreasing its effective resistance. These belts could be reconditioned by baking them for about 24 hours at about $90^{\circ}C$ and treating them with silicone fluid. The belts thus treated showed no further deterioration for a long time even when exposed to normal humid atmospheric conditions.

Table 3.1

Measured surface resistivities of some structural insulating materials

(Room temperature $\sim$ 28°C with a mean relative humidity $\sim$ 60%)

Material	Trade Name	Surface Resistivity ohms/square
Methyl methacrylate	Perspex	6×10^{11}
Nylon	-	$> 10^{14}$
Glass	Pyrex	2×10^{11}
	Index	5×10^{12}
	Corning	1×10^{11}
	S20	5×10^{11}
Glazed Porcelain	-	3×10^{12}
Paper and fibre based laminates	Hylam I	$\sim 10^{10}$
	Hylam II	2.5×10^{8}
	Hylam P116	2×10^{10}
	Hylam P120	3×10^{10}
	Hylam P124	3.5×10^{10}

Table 3.2

Measured surface resistivities of some belt materials

(Room temperature $\sim$ 28°C with a relative humidity $\sim$ 60%)

Material	Trade Name	Surface resistivity ohms/square
Cotton	-	$\sim 10^6$
Rubber (different samples)	-	10^7 to 10^{10}
Neoprene	-	1.5×10^9
Rubberised fabric	-	3.5×10^7 to 1×10^8
Woven nylon belts	Nylastic/Lantilastic	$\sim 10^{12}$

4. Development of a Generating Voltmeter

The generating voltmeter developed by us for monitoring the terminal voltage of the Van de Graaff generator is based on the principle described by Trump, Safford and Van de Graaff (5). It consists essentially of an insulated stator member facing the high voltage terminal from which it is periodically shielded by rotation at constant speed of a grounded sectored disk. The stator to terminal capacitance is thus caused to vary periodically and the induced stator current, which is a measure of the terminal voltage, passes through a special rectifier circuit and is estimated by measuring the voltage drop across a resistance with a vacuum tube voltmeter.

The details of the generating voltmeter are given in fig.4.1 and the principle is shown schematically in the upper portion of fig.4.2. The d.c. output current of the generating voltmeter

$$I = f\left(C_v V - C_s V_R\right) \tag{4.1}$$

where V is the terminal voltage

C_v is the maximum variation of the capacity between the high voltage terminal and the stationary stator

C_s is the value of stator to ground capacitance when the high voltage terminal to stator capacitance is maximum

GENERATING VOLTMETER

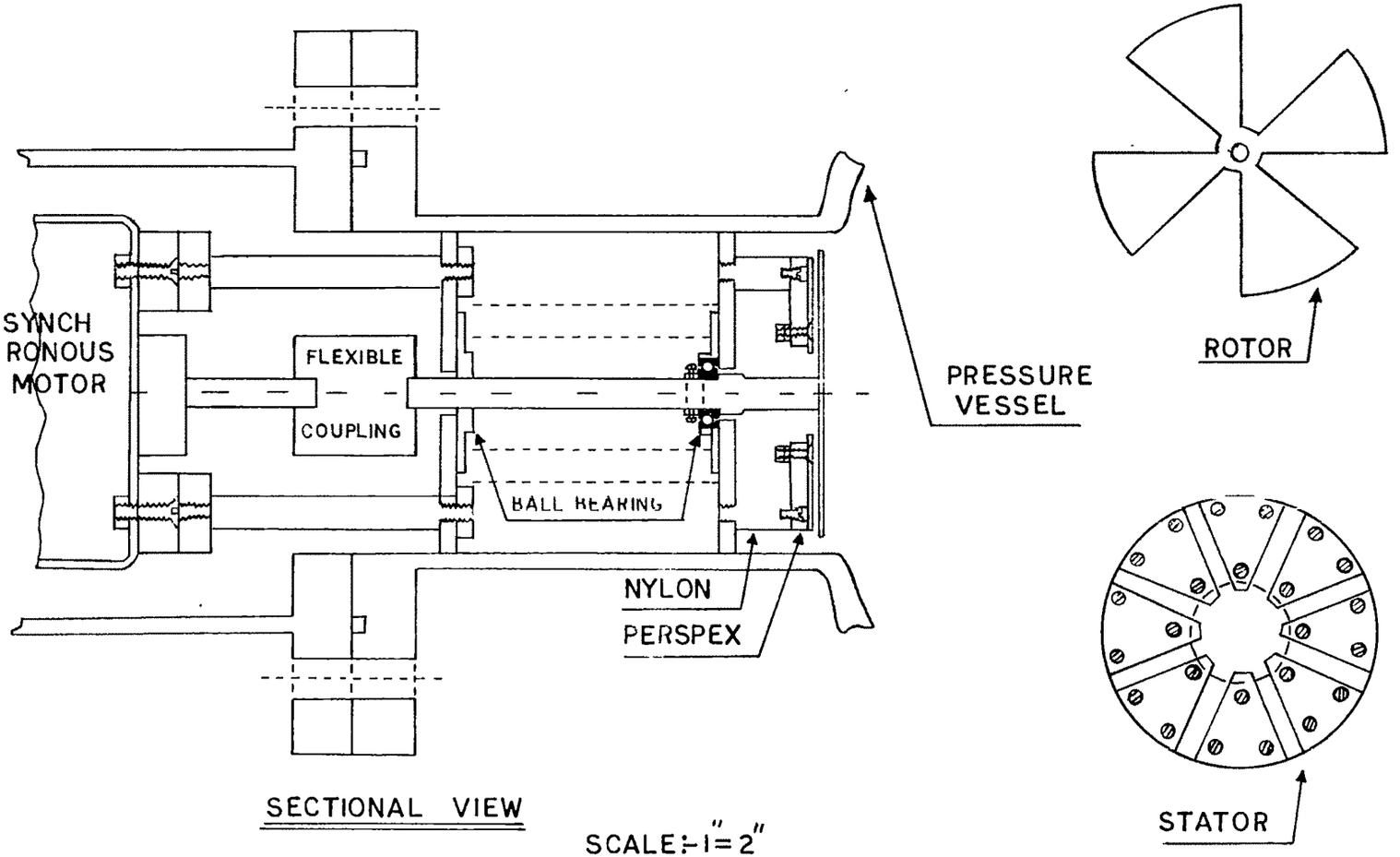

SECTIONAL VIEW

SCALE:- 1" = 2"

FIG. 4.1

f is the effective frequency of variation of the terminal to stator capacitance

and V_R is the reverse bias voltage applied to rectifiers to prevent current flow in the non-conducting part of the cycle

The second term in eqn. (4.1) introduces a small departure from proportionality in the relation between the induced stator current and the terminal voltage. Hence C_s should be kept as small as possible. We have taken special care to ensure that the gap between the stator and rotor remains constant in order to increase the reliability of the voltmeter.

The results of the bench test of our generating voltmeter is shown in fig.4.2. It is seen that the response is essentially linear beyond about 15 KV and that the sensitivity of the voltmeter depends on the position i.e. on the value of the electrostatic field at which it is placed. The generating voltmeter was therefore calibrated under actual operating condition with known voltages applied to the high voltage terminal. The calibration in the low voltage region was done with the help of the spray voltage supply directly connected to the high voltage terminal. Its response was found to be practically independent of pressure and type of the filling gas. The calibration was extended upto about 150 KV with simultaneous terminal voltage measurement by the generating voltmeter, sphere gap and IR drop methods. Above 150 KV to about 1 MV the cross checking was done only through sphere gap measurements. Over the entire region, the linear response of the generating voltmeter was maintained.

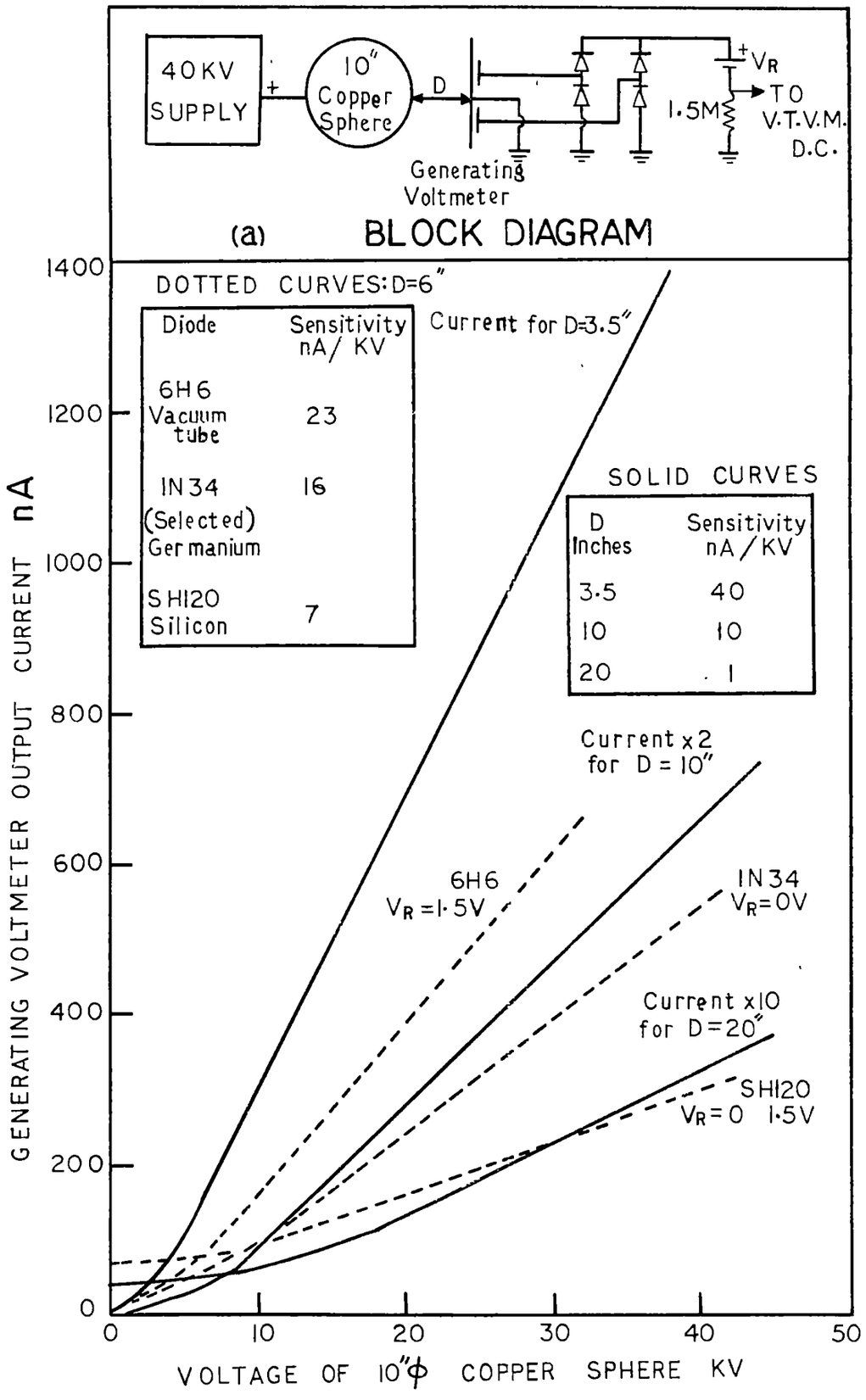

(b) PERFORMANCE DATA

FIG. 4.2

5. Construction of the Pressurised Van de Graaff Generator

The Van de Graaff generator constructed by us is a horizontal machine housed inside a pressure vessel, having an overall dimension of about 3 ft. dia x 5 ft. long. The pressure vessel was fabricated by a local firm according to our specifications and consists of two parts - a 1¼" thick vertical end blocking flange supported on a stand and a movable cylinder having a shell thickness of 5/16". The vertical end blocking flange served as the support for the beam drift tube, accelerating stack, ion source and lens systems and also for the whole of the high voltage terminal cantilever structure system. The movable part of the pressure vessel contained several port holes for the introduction of generating voltmeter, sphere gap assembly and corona needles for high voltage control. The two parts could be coupled to each other through neoprene gasketted joints. The pressure vessel was hydraulically tested at 250 psig, pneumatically tested at about 100 psig and was vacuum tested to about 10^{-2} mm of Hg for several weeks. The pressure vessel can be filled to any desired pressure of nitrogen or any other gas from gas cylinders via hose pipes upto about 100 psig for safe operation.

The high voltage terminal made of 1/16" thick spun aluminium is a 22" dia. cylinder ending as a hemisphere of radius 11" at the top terminal end. It is fixed to a base plate made of 1" thick Al with suitable rounding off at the edges. Perspex was used as the insulating support structure material for the high voltage terminal, the insulation distance between the high voltage

terminal to the ground end base plate being 15". Adequate equipotential rings and field control bars were provided. The gap between the high voltage terminal and the grounded pressure vessel was about 5¾" on the sides and about 11" on the front.

A 18 cm wide x 3 mm thick endless nylon woven charge transport belt was mounted on two 3" dia. solid mild steel rollers, one each at ground and high voltage ends, and was driven by a 3 phase 2 H.P. motor with class E insulation at a linear speed of about 5000 ft/min. The rollers were mounted on self aligning ball bearings with appropriate arrangements for providing proper tensions to the belt. The corona combs for the spraying and collection of charges were made from 1/2" long gramophone needles fixed on a 1/2" dia. brass rod, the distance between two adjacent needles being 1/4".

6. Studies on Charge Transport

Since very little quantitative informations regarding charge transport to the high voltage terminal is available in the literature (6-11), we had to investigate in detail (12) the problem of optimum charge transport with different comb configurations and geometries. The experiments were carried out under atmospheric conditions at a mean room temperature $\sim 28^{\circ}C$ with a mean relative humidity $\sim$ 60%.

For charging and discharging the belt with the help of corona combs, one normally uses one or two combs at the ground end for positive charge spraying and negative charge collection; and one, two or three combs at the high voltage end for positive charge collection and negative charge spraying and their control. We studied various possible arrangements of combs in our set up upto two combs at the ground end and three combs at the high voltage end to find out the relative performances in each case. These comb configurations are represented by the various positions of the four schematic switches of fig.6.1 and are listed in table 6.1.

The explanation of symbols used in fig.6.1 are given below :

C_1, C_2 : Ground end corona combs

V_c : Ground end spray voltage

I_c : Ground end spray current

I_{LC} : Leakage current at the ground end

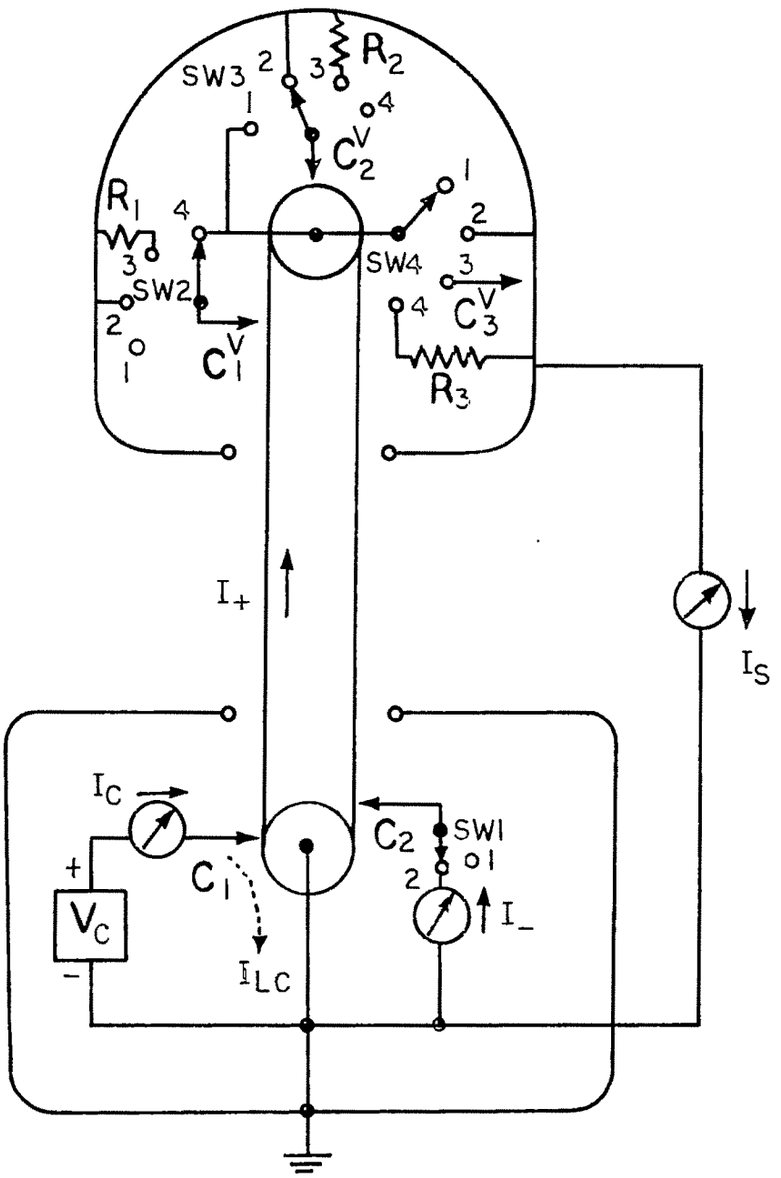

Fig. 6.1 Experimental arrangement for charge transport study.

4318

I_+ : Current due to positive charges going up with the belt

I_- : Current due to negative charges coming down with the belt and collected by the comb C_2

I_s : Short circuit current

C_1^V, C_2^V, C_3^V : Corona combs inside the dome

R_1, R_2, R_3 : Resistances inside the dome

SW1, SW2, SW3, SW4 : Schematic switches

A histogram representing the saturation short circuit currents for different comb configurations with optimum geometries is given in fig.6.2. We obtained a maximum short circuit current $\sim$ 120 μA which corresponds to a charge carrying efficiency $\sim$ 75% of theoretical maximum (9). Of all the configurations studied, configuration IV.2a was found to be the most convenient. It has the advantage of (i) maximum charge transfer under optimum geometrical conditions, (ii) reduced loading on the spray power supply, and (iii) control and stabilization of the roller to dome voltage. This control and stabilization of the roller to dome voltage was achieved through the use of a few additional adjustable needles from the comb C_2^V directed onto the roller without the actual presence of the additional comb C_3^V of configuration V.1 or the resistance R_3 of configuration IV.3.

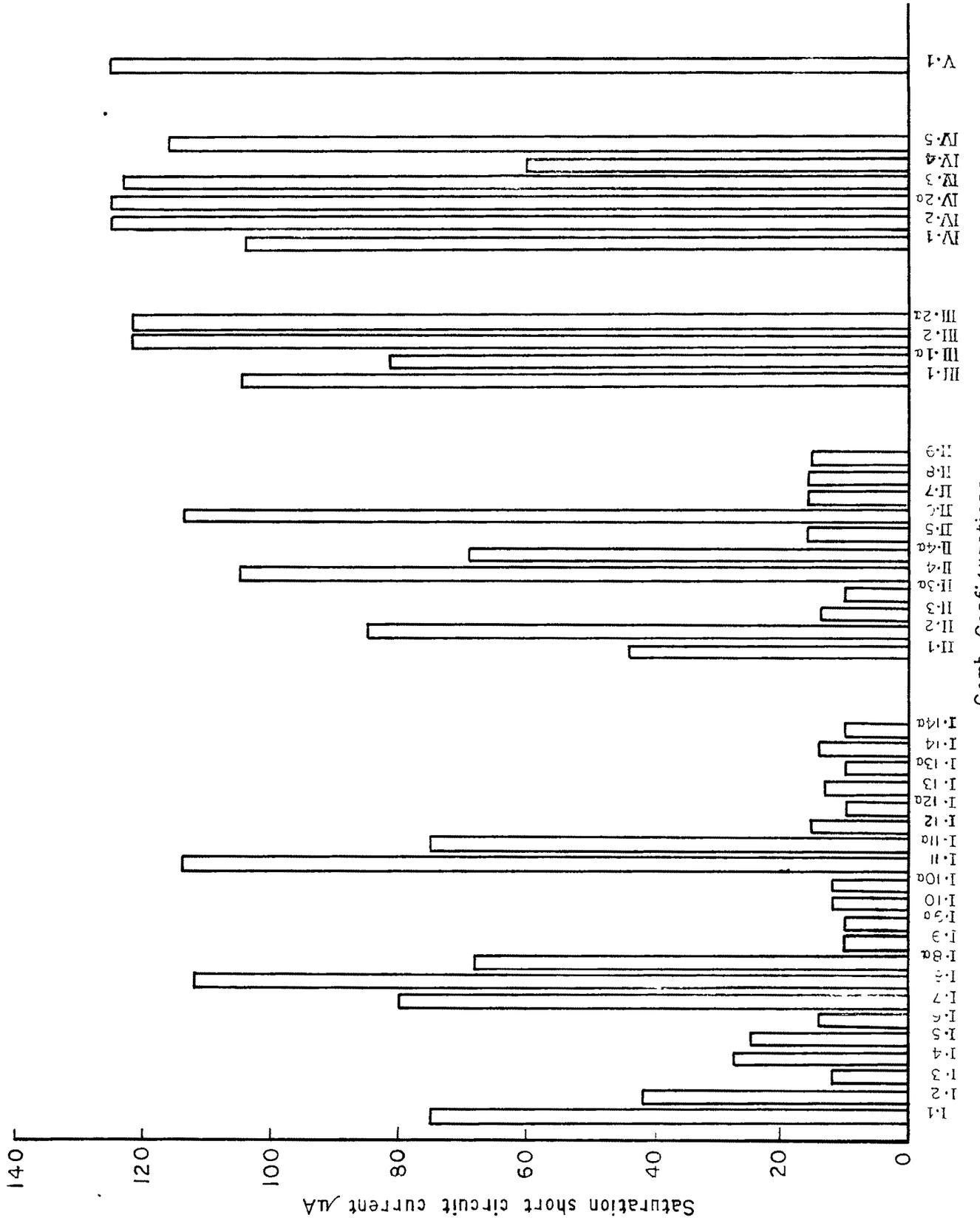

Fig. 6.2 Saturation short circuit currents for different comb configurations.

Table 6.1

Comb configurations studied

Config. No.	Configuration	Config. No.	Configuration
I.1	(1)(2)(4)(1)	I.14	(1)(1)(3)(1)
I.2	(1)(2)(4)(2)	I.14a	(1)(1)(3)(1)Ex
I.3	(1)(3)(4)(1)		
I.4	(1)(4)(4)(4)	II.1	(2)(2)(4)(2)
I.5	(1)(4)(4)(1)	II.2	(2)(2)(4)(1)
I.6	(1)(3)(4)(2)	II.3	(2)(1)(2)(2)
I.7	(1)(2)(4)(4)	II.3a	(2)(1)(2)(2)Ex
I.8	(1)(1)(2)(1)	II.4	(2)(1)(2)(1)
I.8a	(1)(1)(2)(1)Ex	II.4a	(2)(1)(2)(1)Ex
I.9	(1)(1)(2)(2)	II.5	(2)(1)(3)(2)
I.9a	(1)(1)(2)(2)Ex	II.6	(2)(1)(2)(4)
I.10	(1)(1)(3)(2)	II.7	(2)(1)(1)(1)
I.10a	(1)(1)(3)(2)Ex	II.8	(2)(1)(1)(4)
I.11	(1)(1)(2)(4)	II.9	(2)(1)(3)(1)
I.11a	(1)(1)(2)(4)Ex	III.1	(1)(2)(2)(1)
I.12	(1)(1)(1)(1)	III.1a	(1)(2)(2)(1)Ex
I.12a	(1)(1)(1)(1)Ex	III.2	(1)(4)(2)(1)
I.13	(1)(1)(1)(4)	III.2a	(1)(4)(2)(1)Ex
I.13a	(1)(1)(1)(4)Ex		

Table 6.1 (Contd.)

Config. No.	Configuration
IV.1	(2)(2)(2)(1)
IV.2	(2)(4)(2)(1)
IV.2a	(2)(4)(2)(1)Ex
IV.3	(2)(4)(2)(4)
IV.4	(2)(4)(2)(2)
IV.5	(2)(4)(3)(1)
V.1	(2)(4)(2)(3)

Note : 'Config. IV.2a $\equiv$ (2)(4)(2)(1) Ex' means switches SW1, SW2, SW3 and SW4 are respectively in the positions 2,4,2 and 1; and (in cases where 'Ex' is present) there are some adjustable extra needles in the comb C_2^V directed to the roller.

7. Operational Characteristics of the Pressurised Van de Graaff Generator

Although some operational characteristics of Van de Graaff generators under atmospheric conditions are available in the literature through the pioneering works of R. J. Van de Graaff and his associates (6) and of J. F. Smee (7), no such detailed study has been reported in the literature (8-11, 13-15). We, therefore, undertook intensive studies (16) on the operational characteristics of the pressurised Van de Graaff generator constructed by us for a better understanding of its operation.

Commercial quality nitrogen gas (water vapour content $\sim$ 600 ppm), obtained in cylinders from M/s. Indian Oxygen Ltd., was used as the insulating gas. The comb configuration IV.2a was used throughout for studies under pressure. The mean room temperature during the experiments was $\sim 28^{\circ}C$. The terminal voltage was measured by the generating voltmeter. The load current I_{CN} from the high voltage terminal was drawn with the help of an adjustable corona needle assembly which was grounded through a current measuring meter. The gap between the corona needle tip and the dome was varied to control the terminal voltage. When the corona needle touches the dome, the current flowing through it is the short circuit current I_S.

The relation between different currents under short circuit condition shown in figure 6.1, are as follows :

$$I_c = I_+ + I_{LC} \qquad (7.1)$$

and $$I_s = I_+ + I_- \tag{7.2}$$

From these equations we can write

$$I_+ = I_s - I_- \tag{7.3}$$

and $$I_{LC} = I_c - I_+ = I_c + I_- - I_s \tag{7.4}$$

Thus I_+ and I_{LC} were estimated from the measured values of I_c, I_s and I_- under short circuit condition. Also the resultant input current at the ground end

$$I_{in} = I_c + I_- \tag{7.5}$$

and hence can be calculated from the measured values of I_c and I_-.

A plot of the ground end spray current I_c against the spray voltage V_c is an input characteristic of the generator. A typical plot of I_c vs V_c along with the corresponding ground end spraying efficiency I_+/I_c at a nitrogen gas pressure of 3 atmospheres absolute are shown in fig.7.1(a). The spray current increases with the spray voltage. The initial slow rise is due to leakages. The abrupt rise in I_c from $V_c \sim 19$ KV coincides with the threshold of spraying efficiency marking the onset of charge spraying through corona. From here the increase in the spray current and the spraying efficiency is due to the increase in charge density on the belt. The spraying efficiency reaches a peak at $V_c \sim 25$ KV indicating a saturation in the charge density. Subsequent increase in I_c along with the decrease in spraying

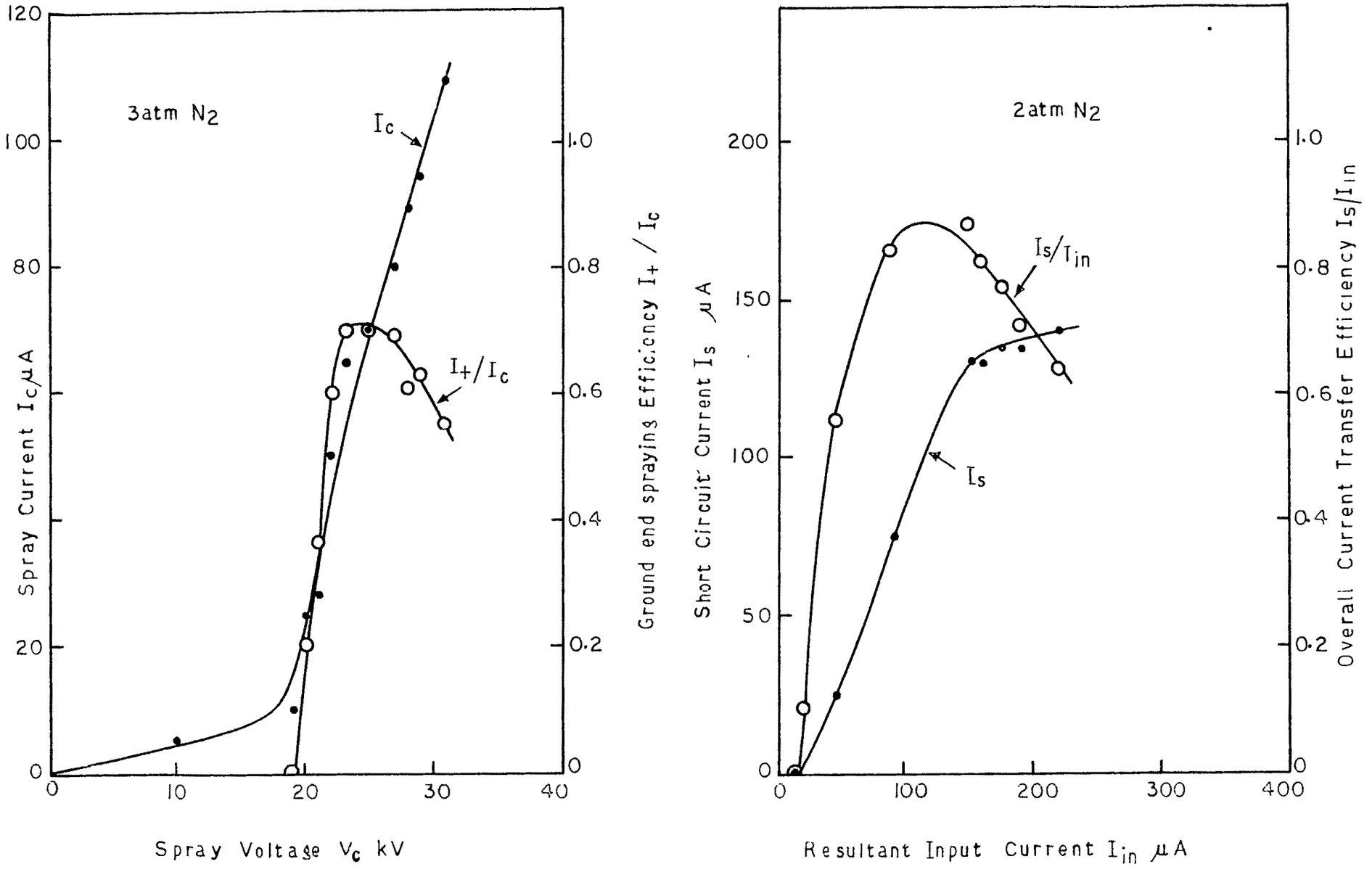
3atm N2
Ic
I+/Ic
Spray Current Ic/μA
Ground end spraying Efficiency I+ / Ic
Spray Voltage Vc kV
(a)
2atm N2
Is/Iin
Is
Short Circuit Current Is μA
Overall Current Transfer Efficiency Is/Iin
Resultant Input Current Iin μA
(b)

FIG. 7.1

efficiency indicates the onset of leakage of charges in excess of saturation from the surface of the belt. Input characteristics at different nitrogen gas pressures upto 6 atmospheres absolute were found to be similar in nature. The threshold for the onset of charge spraying through corona was found to increase linearly with gas pressure - a characteristic feature of the gas breakdown phenomena. The peak ground end spraying efficiency was found to remain constant to a value $\sim$ 70% irrespective of the pressure of nitrogen gas upto 6 atmospheres absolute.

The variation of the short circuit current I_s with the resultant input current I_{in} is a transfer characteristic of the generator. Typical plots of I_s against I_{in} and of overall charge transfer efficiency I_s/I_{in} against I_{in} for a nitrogen gas pressure of 2 atmospheres absolute are shown in fig.7.1(b). The characteristics are similar for different pressures. The maximum overall charge transfer efficiency remains well above 80% and is practically pressure independent indicating that our generator is a low current loss system.

The dependence of the short circuit current I_s, current due to positive charges going up I_+, current due to negative charges coming down I_- and the leakage current at the ground end I_{LC} on the spray current I_c were studied at different nitrogen gas pressures under short circuit condition. A typical plot for 3 atm, N_2 is shown in fig.7.2(a). The currents I_s, I_+ and I_- all show saturation with I_c. The leakage current I_{LC} increases rapidly after saturation in I_+ is attained. The linear increase

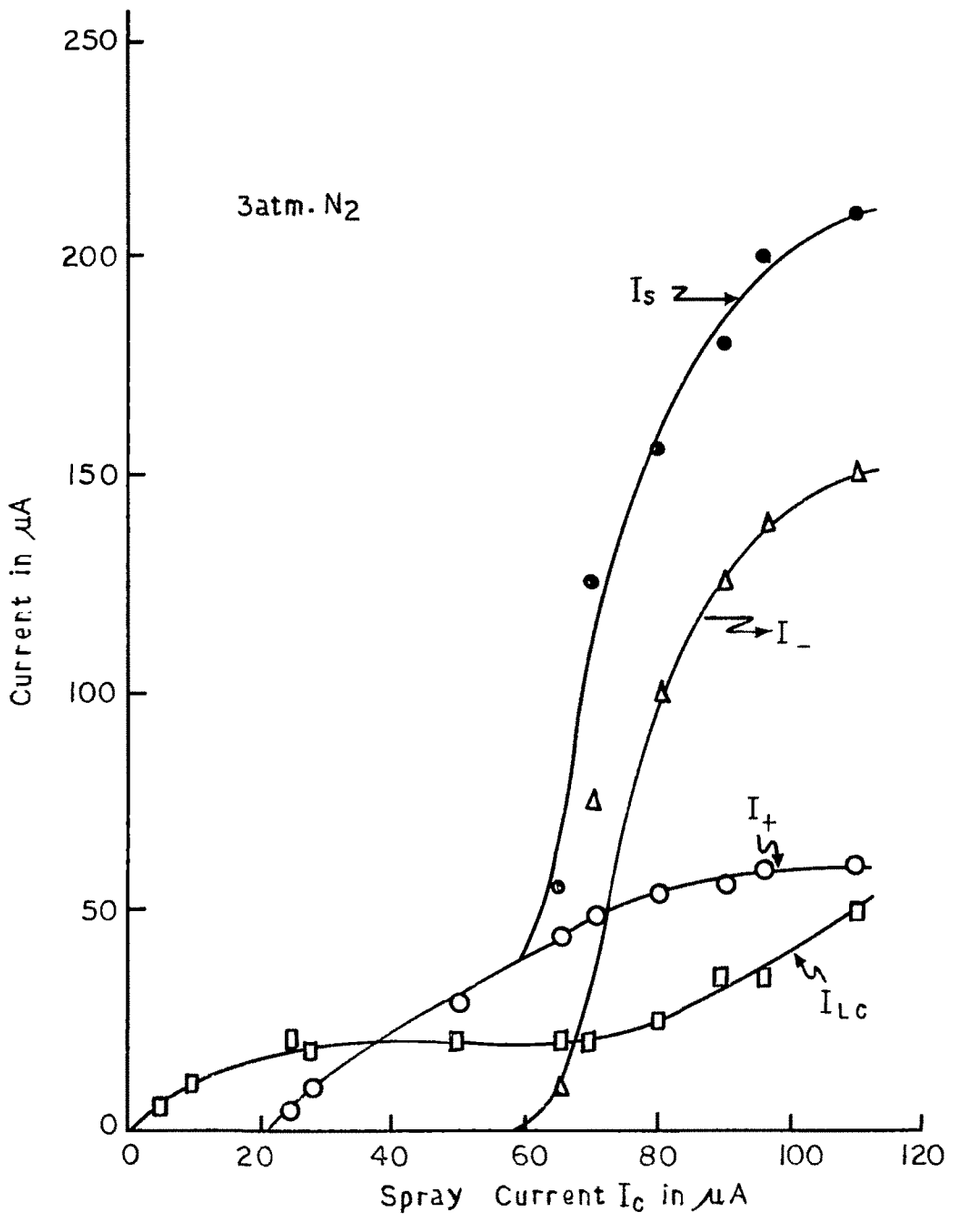
3atm. N_2
I_s
I_-
I_+
I_{LC}
Current in μA
Spray Current I_c in μA
0
50
100
150
200
250
0
20
40
60
80
100
120

(a)

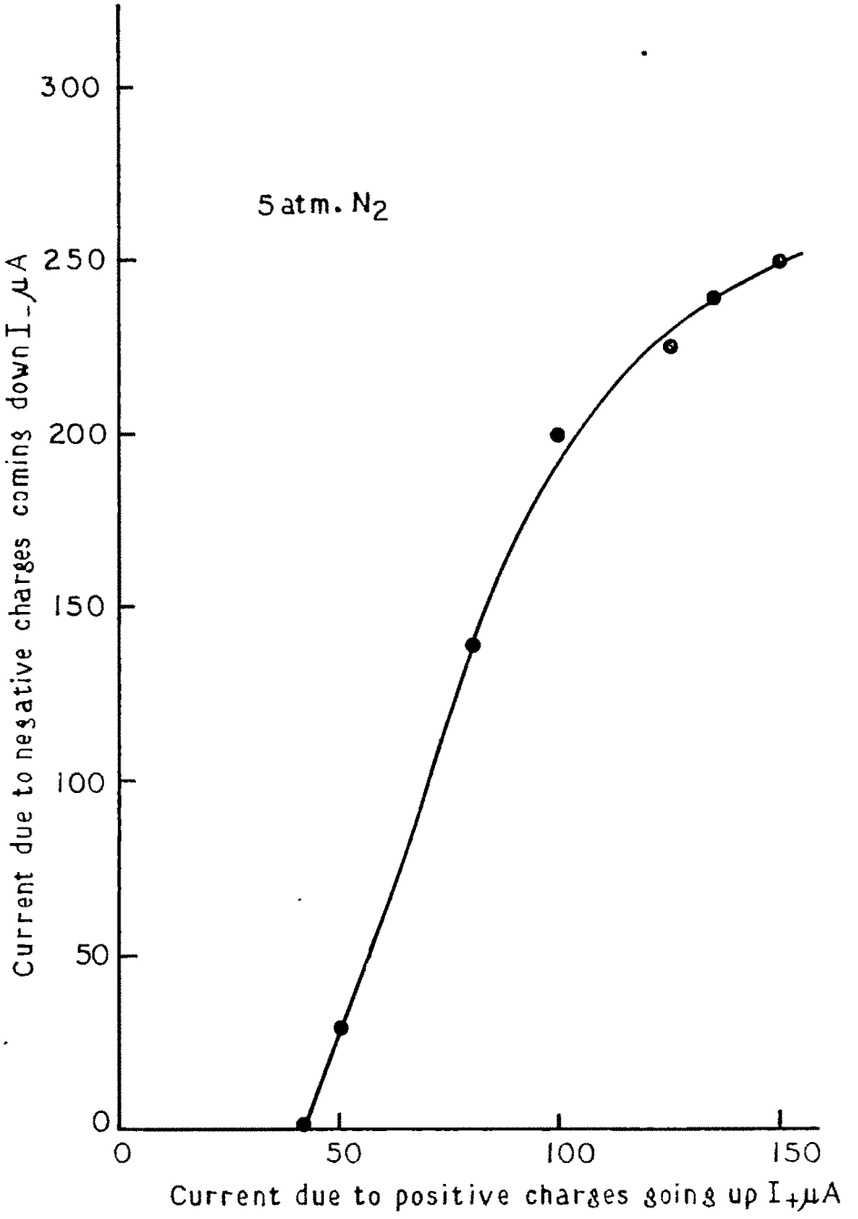
5 atm. N_2
Current due to negative charges coming down I_- μA
Current due to positive charges going up I_+ μA
0
50
100
150
200
250
300
0
50
100
150

(b)

FIG. 7.2

in the saturation values of I_s, I_+ and I_- with nitrogen gas pressure is shown in fig.7.3. The systematic difference in the saturation values of I_+ and I_- seems to be due to different sticking probabilities of different types of ions onto the charge transport belt.

The current due to negative charges coming down I_- as a function of the current due to positive charges going up I_+ was studied at different nitrogen gas pressures. A typical curve for 5 atm. N_2 is shown in fig.7.2(b). There is a threshold value of I_+ from where I_- starts and this threshold value was found to increase linearly with nitrogen gas pressure. At a particular pressure the threshold value of I_+ is the minimum amount of up-going positive charge current that is necessary to produce the required roller to dome voltage for negative charge spraying to commence. I_- ultimately shows saturation with I_+ due to saturation in the negative charge density on the belt.

The maximum steady terminal voltages attained in our Van de Graaff generator at different nitrogen gas pressure$^{\Delta}_{\Lambda}$ are shown in fig.7.3. A maximum terminal voltage of 1.1 million volt was achieved at a nitrogen gas pressure of 6 atmospheres absolute with a spray voltage of 38 KV. The load characteristics of the generator at different nitrogen gas pressures are shown in fig.7.4. The curves reveal the essentially constant current feature of the generator.

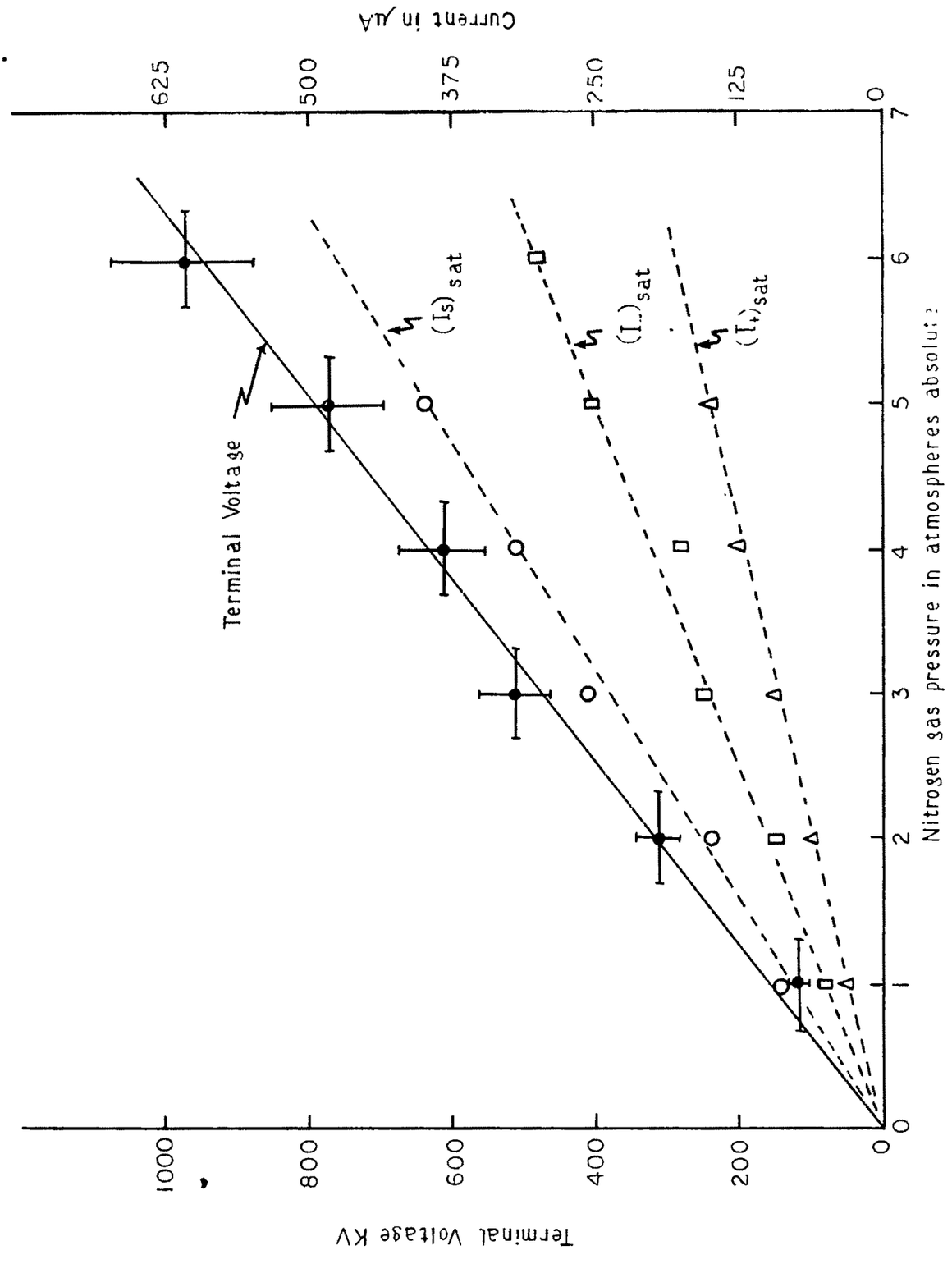

Fig. 7.3 Dependence of terminal voltage and the saturation values of the currents I_s, I_+ & I_- on nitrogen gas pressure.

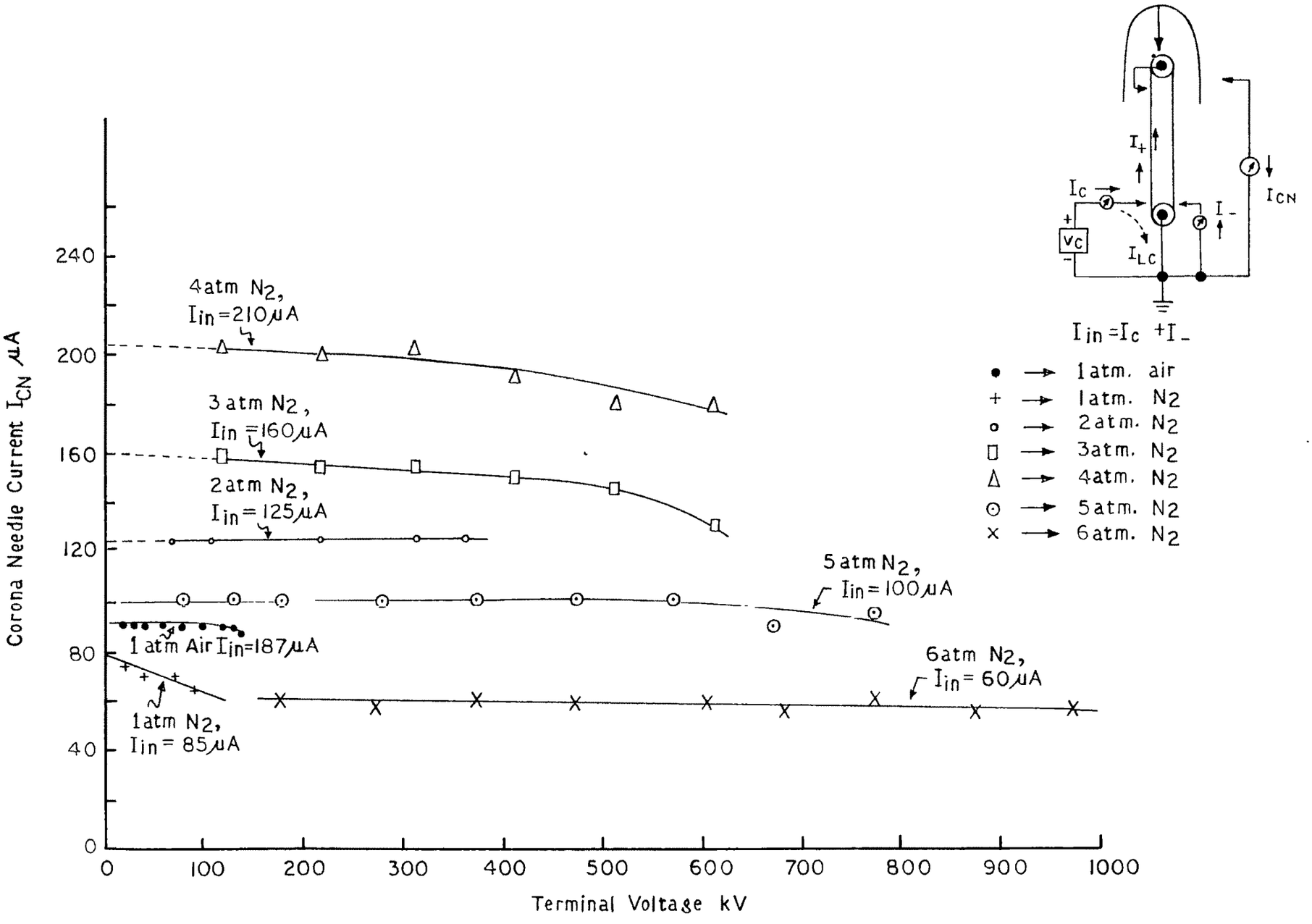

Fig. 7.4 Load characteristics of the Van de Graaff generator at different gas pressures.

8. Operation as a Test Accelerator

In order to operate the Van de Graaff generator as a test accelerator, we had to additionally incorporate (i) a high vacuum system capable of producing a vacuum $\sim 1 \times 10^{-5}$ mm of Hg under operating conditions, (ii) accelerating stack, and (iii) ion source assembly along with its power feeding system.

The vacuum assembly consists of a 6" oil diffusion pump backed by a 300 litres/min. mechanical pump. Proper liquid nitrogen traps were provided on top of both the mechanical and the diffusion pump. It could handle a gas feed rate $\sim$ 10 atmospheric c.c./hour while maintaining a vacuum $\sim 1 \times 10^{-5}$ mm of Hg. RCA 1946 thermocouple gauge, RCA 1949 ionization gauge and Edwards Penning gauge were used to measure vacuum.

The accelerating stack constructed by us consists of 10 sections of Index glass rings (each 5¼" o.d./4" i.d. x 1¼" long) and 9" dia x 1/2" thick aluminium plates with 2" dia. central hole interposed between the glass rings. Special care was taken to make the Index glass rings strain free. The aluminium plates were first degreased and then bonded to the glass rings using the epoxy resin Araldite (ICI brand) at room temperature to form the accelerating stack.

Electric power inside the high voltage terminal was generated by a 800 W, 110 V, 400 Hz alterator coupled to the high voltage end roller with a V-belt. The RF oscillator (using

829B twin triode in push-pull arrangement and capable of delivering 60 W at 80 MHz), the oscillator power supply (500-700 V, 200 mA), the oscillator filament supply (6.3 V a.c., 3A), probe voltage supply (0-5 KV, 10 mA), focussing voltage supply (0-15 KV, 1 mA), magnet power supply (12 V, 1 A) were designed, fabricated and installed inside the high voltage terminal. We designed and constructed the 400 Hz transformers and variacs ourselves as the commercial ones could not be fitted in the small space available within the high voltage terminal of our accelerator. A RF ion source with a 4" long bottle and a Gap-cum-Einzel beam focussing lens system was set up on the high voltage side of the accelerating stack. The control variacs of the probe and focussing supplies and the fine control needle valve regulating the gas flow rate to the ion source could be remote controlled from outside the pressure vessel through perspex shafts fitted with synchromotors placed at the ground end.

Under test runs at low current levels we could obtain a focussed beam of deuterons as seen on a glass plate at the end of the beam drift tube. The beam current when measured by a biased Faraday cup was found to be $\sim$ 50 μA.

References

PART A

Design-Studies of a Van de Graaff Accelerator

1. K. W. Allen, in Nuclear Spectroscopy and Reactions Part A p.3 (ed. J. Cerny, Academic Press, 1974).

2. D. A. Bromley, Nucl. Instr. & Meth., 122 (1974) 1.

3. R. J. Van de Graaff, Phys. Rev., 38 (1931) 1919.

4. A. K. Ganguly and A. Saha, Proc. National Symposium on Radiation Physics, Mysore, India, 1976 ~~(In Press)~~; Jour. Mysore Univ. (India) B26 (1977) 54 (Diamond Jubilee Special Issue).

5. J. G. Trump, F. J. Safford and R. J. Van de Graaff, Rev. Sci. Instr., 11 (1940) 54.

6. L. C. Van Atta, D. L. Northrup, C. M. Van Atta and R. J. Van de Graaff, Phys. Rev., 49 (1936) 761.

7. J. F. Smee, J. Inst. Elect. Engrs., Pt.1, 91 (1944) 422.

8. R. J. Van de Graaff, J. G. Trump and W. W. Buechner, Rep. Prog. Phys., 11 (1946) 1.

9. J. D. Craggs and J. M. Meek, High Voltage Laboratory Technique, pp. 37-53 (Butterworths Scientific Publications, London, 1954).

10. R. G. Herb, Handbuch der Physik, 44 (1959) 64.

11. M. S. Livingston and J. P. Blewett, Particle Accelerators (McGraw-Hill, 1962).

12. A. K. Ganguly and A. Saha, Ind. J. Phys., 49 (1975) 287.

13. J. G. Trump and R. J. Van de Graaff, Phys. Rev., 55 (1939) 1160.

14. J. G. Trump, Nucl. Instr. & Meth., 28 (1964) 10.

15. R. G. Herb, D. B. Parkinson and D. W. Kerst, Phys. Rev., 51 (1937) 75.

16. A. K. Ganguly and A. Saha, Ind. J. Phys., 50 (1976) 683.

17. M. A. Tuve, L. R. Hofstad and O. Dahl, Phys. Rev., 48 (1935) 315.

18. K. W. Allen, F. A. Julian, W. D. Allen, A. E. Pyrah and J. Blears, Nature, 184 (1959) 303.

19. R. J. Van de Graaff, Nucl. Instr. & Meth., 8 (1960) 195.

20. T. W. Aitken, B. S. Halliday, W. T. Johnstone, C. W. Jones, T. Joy, M. C. Morris, N. R. S. Tait and R. G. P. Voss, Nucl. Instr. & Meth., 122 (1974) 235.